

# Collisional Damping of Giant Monopole and Quadrupole Resonances

S. Yildirim<sup>1</sup>, A. Gokalp<sup>1</sup>, O. Yilmaz<sup>1</sup> and S. Ayik<sup>2</sup>

<sup>1</sup> *Physics Department, Middle East Technical University,*  
06531 Ankara, Turkey

<sup>2</sup> *Physics Department, Tennessee Technological University, Cookeville TN 38505, USA*

(November 21, 2018)

## Abstract

Collisional damping widths of giant monopole and quadrupole excitations for  $^{120}\text{Sn}$  and  $^{208}\text{Pb}$  at zero and finite temperatures are calculated within Thomas-Fermi approximation by employing the microscopic in-medium cross-sections of Li and Machleidt and the phenomenological Skyrme and Gogny forces, and are compared with each other. The results for the collisional widths of giant monopole and quadrupole vibrations at zero temperature as a function of the mass number show that the collisional damping of giant monopole vibrations accounts for about 30–40% of the observed widths at zero temperature, while for giant quadrupole vibrations it accounts for only 20–30% of the observed widths of zero temperature.

PACS:24.30.Cz, 24.30.Gd, 25.70.Ef, 25.70.Lm

Typeset using REVTeX

Nuclear collective vibrations built on the ground state and on the excited states of the nucleus have been studied extensively during the last several years both theoretically and experimentally [1]. On the theoretical side, much effort have been devoted to understand the damping properties of giant dipole excitations at zero and finite temperatures. In medium-weight and heavy nuclei at relatively low temperatures the damping results mostly from the spreading width  $\Gamma^\downarrow$  which is due to mixing of the collective state with the near by more complex doorway states [2–4]. There are essentially two different approaches for calculation of the spreading widths: (i) Coherent mechanism due to coupling with low-lying surface modes which provides an important mechanism for damping of giant resonance in particular at low temperatures [5–8], (ii) Damping due to the coupling with incoherent 2p-2h states which is usually referred to as the collisional damping [9–12], and the Landau damping modified by two-body collisions [13–15]. The investigations carried out on the basis of these approaches have been partially successful in explaining the broadening of the giant dipole resonance with increasing temperature. In this work, we do not consider the coherent contribution to damping, but investigate the collisional damping of isoscalar giant monopole and isoscalar giant quadrupole resonances at zero and finite temperatures due to decay of the collective state into incoherent 2p-2h excitations in the basis of a semi-classical non-Markovian transport approach. In this approach, the collisional term involves two-body transition rates which can be expressed in terms of the in-medium scattering cross sections [10]. Therefore in order to assess the contribution of collisional damping to the total width of giant resonance excitations, we need realistic in-medium cross-sections which correctly interpolate between the free space and the medium. In previous investigations, the contributions of spreading width resulting from the decay of the collective state into incoherent 2p-2h states have been estimated by employing either free nucleon-nucleon cross sections or an effective Skyrme force [9,10]. However, Skyrme force at most can provide a semiquantitative description of the collisional damping since it provides a poor approximation in the collisional term because in the vicinity of nuclear surface it does not match at all to the free nucleon-nucleon cross-sections. In a recent work, we calculated the collisional damping width of the giant dipole excitations

by employing the microscopic in-medium cross sections of Li and Machleidt [16], which interpolate correctly between the free space and the medium and provide the best available input for determining the magnitude of the collisional damping [17]. In the present work, we extend this analysis to the study of the collisional damping widths of giant monopole and quadrupole excitations by employing the microscopic in-medium cross-sections of Li and Machleidt and phenomenological Skyrme and Gogny forces.

We study the collective vibrations in the small amplitude limit of the extended TDHF theory in which damping resulting from the coupling of the collective state to incoherent 2p-2h states is included in the form of a non-Markovian collision term [18,19]. In the Hartree-Fock representation, the Fourier transform of the self-energy of collective modes due to coupling with the incoherent 2p-2h states is given by

$$\Sigma_{\lambda}(\omega) = \frac{1}{4} \sum \frac{|\langle ij|[O_{\lambda}^{\dagger}, v]|kl \rangle_A|^2}{\hbar\omega - \Delta\epsilon + i\eta} [n_k n_l \bar{n}_i \bar{n}_j - n_i n_j \bar{n}_k \bar{n}_l] \quad (1)$$

where  $O_{\lambda}^{\dagger}$  is the collective operator associated with the RPA mode  $\lambda$ ,  $v$  is the effective interaction that couples the ph-space with 2p-2h configurations,  $\bar{n}_i = 1 - n_i$ ,  $\Delta\epsilon = \epsilon_i + \epsilon_j - \epsilon_k - \epsilon_l$ , and  $\eta$  is a small positive number [10]. The real and imaginary parts of the self energy,  $\Sigma_{\lambda}(\omega) = \Delta_{\lambda}(\omega) - \frac{i}{2}\Gamma_{\lambda}(\omega)$ , determine the energy shift and the damping width of the collective excitation, respectively [3].

We evaluate the expression for the self-energy in the Thomas-Fermi approximation, which corresponds to the semi-classical transport description of the collective vibrations. In Thomas-Fermi approximation the self-energy of the collective modes can be deduced from the quantal expression (1) by replacing the occupation numbers  $n_i$  with the equilibrium phase-space density given by the Fermi-Dirac function as  $n_i \rightarrow f(\epsilon, T) = 1/[\exp(\epsilon - \mu)/T + 1]$  with  $\mu$  denoting the chemical potential, and summations over the 2p-2h states with integrals over phase-space,  $\Sigma \rightarrow \int d\mathbf{r} d\mathbf{p}_1 d\mathbf{p}_2 d\mathbf{p}_3 d\mathbf{p}_4$  [10,20]. Furthermore, spin-isospin effects in collective vibration can be incorporated into the treatment by considering proton and neutron degrees of freedom separately. Observing that in isoscalar modes protons and neutrons vibrate in phase, in Thomas-Fermi approximation the collisional widths of isoscalar modes

can be expressed as [10]

$$\Gamma_\lambda^s = \frac{1}{N_\lambda} \int d\mathbf{r} d\mathbf{p}_1 d\mathbf{p}_2 d\mathbf{p}_3 d\mathbf{p}_4 [W_{pp} + W_{nn} + 2W_{pn}] \frac{(\Delta\chi_\lambda)^2}{2} Z f_1 f_2 \bar{f}_3 \bar{f}_4 \quad (2)$$

where  $N_\lambda = \int d\mathbf{r} d\mathbf{p} (\chi_\lambda)^2 (-\frac{\partial}{\partial \epsilon} f)$  is a normalization,  $\Delta\chi_\lambda = \chi_\lambda(1) + \chi_\lambda(2) - \chi_\lambda(3) - \chi_\lambda(4)$ ,  $Z = [\delta(\hbar\omega_\lambda - \Delta\epsilon) - \delta(\hbar\omega_\lambda + \Delta\epsilon)]/\hbar\omega_\lambda$ , and  $\chi_\lambda(t)$  denotes the distortion factor of the phase-space density  $\delta f(t) = \chi_\lambda(t)(-\partial f/\partial \epsilon)$  in the corresponding mode. In this expression, two-body transition rates  $W_{pp}$ ,  $W_{nn}$  and  $W_{pn}$  associated with proton-proton, neutron-neutron and proton-neutron collisions are given in terms of the corresponding scattering cross-sections

$$W(12; 34) = \frac{1}{(2\pi\hbar)^3} \frac{4\hbar}{m^2} \frac{d\sigma}{d\Omega} \delta(\mathbf{p}_1 + \mathbf{p}_2 - \mathbf{p}_3 - \mathbf{p}_4). \quad (3)$$

We apply the formula (2) to calculate the collisional widths of monopole and quadrupole vibrations. We use the nuclear fluidynamical model to express the distortion factors of the momentum distribution in which the distortion factors can be expressed in terms of the velocity field  $\Phi(\mathbf{r})$  associated with the collective mode as  $\chi = (\mathbf{p} \cdot \nabla)(\mathbf{p} \cdot \nabla)\Phi(\mathbf{r})$ . An accurate description of the monopole vibrations can be obtained by parameterizing the velocity field in terms of the zeroth order Bessel functions  $\Phi(r) = j_0(kr)$ , with the wave number  $k = \pi/R$ , and the nuclear radius  $R$  [21,22]. For the quadrupole vibrations, we use the parameterization of the velocity field in terms of second order Bessel function  $\Phi(r) = j_2(kr)$  and take  $k = 3.34/R$  [23]. We also carry out the calculations for the collisional width of the quadrupole vibrations by taking the distortion factor of the momentum distribution according to the scaling picture as  $\chi_Q = p^2 P_2(\cos\theta)$  [10]. In the case of isoscalar modes, the collisional width is determined by the spin-isospin averaged nucleon-nucleon cross-section,  $(d\sigma/d\Omega)_0 = [(d\sigma/d\Omega)_{pp} + (d\sigma/d\Omega)_{nn} + 2(d\sigma/d\Omega)_{pn}]/4$ . The nucleon-nucleon cross-sections in this expression associated with an effective residual interaction can be expressed as

$$\left(\frac{d\sigma}{d\Omega}\right)_{pp} = \left(\frac{d\sigma}{d\Omega}\right)_{nn} = \frac{\pi}{(2\pi\hbar)^3} \frac{m^2}{4\hbar} \frac{1}{4} \sum_S (2S+1) | \langle \mathbf{q}; S, T = 1 | v | \mathbf{q}'; S, T = 1 \rangle_A |^2 \quad (4)$$

and

$$\left(\frac{d\sigma}{d\Omega}\right)_{pn} = \frac{\pi}{(2\pi\hbar)^3} \frac{m^2}{4\hbar} \frac{1}{8} \sum_{S,T} (2S+1) | \langle \mathbf{q}; S, T | v | \mathbf{q}'; S, T \rangle_A |^2, \quad (5)$$

where  $\mathbf{q} = (\mathbf{p}_1 - \mathbf{p}_2)/2$ ,  $\mathbf{q}' = (\mathbf{p}_3 - \mathbf{p}_4)/2$  are the relative momenta before and after a binary collision, and  $\langle \mathbf{q}; S, T | v | \mathbf{q}'; S, T \rangle_A$  represents the fully anti-symmetric matrix element of the residual interaction between two particle states with total spin and isospin  $S$  and  $T$ . By noting that,  $S=T=1$  and  $S=T=0$  matrix elements of the interaction are space antisymmetric, and  $S=1, T=0$  and  $S=0, T=1$  matrix elements are space symmetric, we find that the spin-isospin averaged nucleon-nucleon cross-section associated with the Gogny force is given by

$$\begin{aligned} \left( \frac{d\sigma}{d\Omega} \right)_0^G &= \frac{\pi}{(2\pi\hbar)^3} \frac{m_G^{*2}}{4\hbar} \frac{1}{8} \\ &\times \left\{ \frac{9}{2} \left| \sum_{i=1}^2 I_i^-(W_i + B_i - H_i - M_i) \right|^2 + \frac{1}{2} \left| \sum_{i=1}^2 I_i^-(W_i - B_i + H_i - M_i) \right|^2 + \right. \\ &\quad \left. \frac{3}{2} \left| \sum_{i=1}^2 I_i^+(W_i + B_i + H_i + M_i) + 4t_3\rho^{1/3} \right|^2 + \frac{3}{2} \left| \sum_{i=1}^2 I_i^+(W_i - B_i - H_i + M_i) \right|^2 \right\} \quad (6) \end{aligned}$$

where  $m_G^*$  denotes the effective mass corresponding to the Gogny force, and the quantities  $I_i^+$  and  $I_i^-$  are the symmetric and anti-symmetric matrix elements of the Gaussian factor in the force,

$$I_i^\pm = (\sqrt{\pi}\mu_i)^3 \left( \exp\left[-\frac{1}{4}(\mathbf{q} - \mathbf{q}')^2 \left(\frac{\mu_i}{\hbar}\right)^2\right] \pm \exp\left[-\frac{1}{4}(\mathbf{q} + \mathbf{q}')^2 \left(\frac{\mu_i}{\hbar}\right)^2\right] \right). \quad (7)$$

In these expressions,  $\rho$  is the local density and  $W_i, B_i, H_i, M_i, \mu_i$  denote the standard parameters of the Gogny force [24,25]. In a similar manner, this cross-section can be calculated in terms of the effective Skyrme force as [10,17]

$$\begin{aligned} \left( \frac{d\sigma}{d\Omega} \right)_0^S &= \frac{\pi}{(2\pi\hbar)^3} \frac{m_S^{*2}}{4\hbar} \left( \frac{3}{4} [t_0(1-x_0) + \frac{t_1}{2\hbar^2}(1-x_1)(\mathbf{q}^2 + \mathbf{q}'^2) + \frac{t_3}{6}(1-x_3)\rho^\alpha]^2 + \right. \\ &\quad \frac{3}{4} [t_0(1+x_0) + \frac{t_1}{2\hbar^2}(1+x_1)(\mathbf{q}^2 + \mathbf{q}'^2) + \frac{t_3}{6}(1+x_3)\rho^\alpha]^2 + \\ &\quad \left. \frac{5}{8} \left[ \left(\frac{t_2}{\hbar^2}\right)^2 (1-x_2)^2 + 3 \left(\frac{t_2}{\hbar^2}\right)^2 (1+x_2)^2 \right] (\mathbf{q} \cdot \mathbf{q}')^2 \right). \quad (8) \end{aligned}$$

The expressions for the effective masses  $m_G^*(r)$  and  $m_S^*(r)$  for the Gogny and Skyrme forces are given in [24,25]. The angle  $\Theta$  between  $\mathbf{q}$  and  $\mathbf{q}'$  in the cross-sections (6) and (8) defines the scattering angle in the center of mass frame, and the total cross-section is found by an integration over this angle,  $\sigma_0 = 2\pi \int \sin\Theta d\Theta (d\sigma/d\Omega)_0$ . Microscopic in-medium cross-

sections of Li and Machleidt [16] for proton-proton and neutron-proton cross-sections are parameterized as

$$\sigma_{pp}^{LM} = [23.5 + 0.00256 (18.2 - E_{lab}^{0.5})^{4.0}] \frac{1.0 + 0.1667 E_{lab}^{1.05} \rho^3}{1.0 + 9.704 \rho^{1.2}} , \quad (9)$$

$$\sigma_{pn}^{LM} = [31.5 + 0.092 |20.2 - E_{lab}^{0.53}|^{2.9}] \frac{1.0 + 0.0034 E_{lab}^{1.51} \rho^2}{1.0 + 21.55 \rho^{1.34}} , \quad (10)$$

where  $E_{lab} = (\mathbf{p}_1 - \mathbf{p}_2)^2/2m = 2\mathbf{q}^2/m$  is the kinetic energy of the projectile in the rest frame of the target nucleon which is also equal to twice the energy available in the center of mass frame.

In figure 1 and figure 2, we compare the spin-isospin averaged nucleon-nucleon cross-sections calculated using the microscopic in-medium cross-sections of Li and Machleidt (dotted lines) with the cross-sections of the Gogny force (dashed lines) and the Skyrme force (solid lines) with SkM\* parameters. In figure 1, the total cross-sections are plotted as a function of the projectile energy  $E_{lab}$  at two different nuclear matter densities  $\rho = \rho_0 = 0.18 \text{ fm}^{-3}$  (top panel) and  $\rho = \rho_0/2$  (bottom panel). The cross-sections shown in the left and right parts of the figure are calculated with the bare nucleon mass and the corresponding effective masses, respectively. Around the normal nuclear matter density  $\rho \approx \rho_0$ , and over a narrow energy interval around 150 MeV, these cross-sections roughly match, however at lower densities and at lower and higher energies the phenomenological cross-sections deviate strongly from the microscopic cross-sections, deviations being larger in the calculations with the bare nucleon mass. In figure 2, the cross-sections are shown as a function of density for the bombarding energy  $E_{lab} = 100 \text{ MeV}$ . The microscopic calculations approach the free nucleon-nucleon cross-section for decreasing density, on the other hand the phenomenological cross-sections strongly increase and reach large values in free space. Therefore, we can safely state that the microscopic calculations of Li and Machleidt provide a more reliable description of the in-medium cross-sections than those given by the finite range Gogny and the zero range Skyrme force. In a previous work [17], the momentum integrals in the expression for the damping width of giant dipole resonance were evaluated ex-

actly. We follow the same method in the present work and evaluate the momentum integrals in the expression (2) exactly for monopole and quadrupole vibrations. In this calculation the angular anisotropy of the cross-sections are neglected and we make the replacement  $(d\sigma/d\Omega)_0 \rightarrow \sigma_0/4\pi$ . In the numerical evaluations, we determine the nuclear density  $\rho(r)$  in Thomas-Fermi approximation using a Wood-Saxon potential with a depth  $V_0 = -44$  MeV, thickness  $a = 0.67$  fm and sharp radius  $R_0 = 1.27A^{1/3}$  fm, and we calculate the position dependent chemical potential  $\mu(r, T)$  in the Fermi-Dirac function  $f(\epsilon, T)$  at each temperature. We use the formula  $\hbar\omega = 64A^{-1/3}$  MeV for the giant quadrupole resonance energies, and the expressions  $\hbar\omega = 31.2A^{-1/3} + 20.6A^{-1/6}$  MeV for  $A \geq 70$  and  $\hbar\omega = 17.5$  MeV for  $A < 70$  to calculate the giant monopole resonance energies. Figure 3 shows the collisional damping width of giant monopole resonance in  $^{120}\text{Sn}$  and  $^{208}\text{Pb}$  as a function of temperature. In figure 4, we show the collisional damping width of giant quadrupole resonance in  $^{120}\text{Sn}$  and  $^{208}\text{Pb}$  as a function of temperature, where we use the distortion factors of momentum distributions obtained from the fluidynamical model by the parametrization  $\Phi(r) = j_2(kr)$  of the velocity field. The collisional damping widths of the same nuclei calculated by employing the distortion factor  $\chi_Q = p^2 P_2(\cos\theta)$  using scaling approximation are shown in figure 5. In these figures T=0 experimental data points are also indicated. Calculations performed with the cross-sections of Li and Machleidt are denoted with dotted lines. For comparison, we also show the results with the SkM\* (solid lines) and the Gogny (dashed lines) cross-sections with the bare nucleon mass (lower panel) and the effective nucleon mass (upper panel). For both monopole and quadrupole vibrations, the calculations with cross-sections of Li and Machleidt exhibit a weaker temperature dependence than the calculations with the SkM\* and the Gogny cross-sections with the bare nucleon mass and result in considerably smaller damping widths at all temperatures than those with the cross-sections of the phenomenological forces. However, if the effective nucleon mass is used, the calculations employing microscopic and phenomenological cross-sections give collisional damping widths that almost agree with each other at low temperatures with differences becoming somewhat more appreciable only at high temperatures. Furthermore, a comparison of figure 4 and figure 5

shows that the calculations for quadrupole vibrations employing the scaling approximation for the distortion factors result in smaller values for the damping width as a function of temperature than those where the distortion factors are determined from fluidynamical picture. Moreover, in calculations using the effective nucleon mass, scaling approximation for the distortion factors give results for the collisional damping widths that become somewhat more appreciably different for microscopic and phenomenological cross-sections at relatively high temperatures. In figure 6, we show the collisional damping widths of giant monopole (left) and quadrupole vibrations (right) as a function of the mass number at zero temperature calculated with the microscopic cross-sections (dotted lines), and with the SkM\* (solid lines) and the Gogny (dashed lines) cross-sections. Here, we use the effective nucleon mass and employ the scaling approximation for distortion factors in quadrupole vibrations, since at zero temperature both scaling and fluidynamical pictures for distortion factors give results that are not appreciably different from each other. If we base our conclusion on the result obtained employing the microscopic in-medium cross-sections, we can conclude that the collisional damping of giant monopole vibrations accounts for about 30 – 40% of the observed widths at zero temperature, while for giant quadrupole vibrations it accounts for only 20 – 30% of the observed widths at zero temperature.

### **Acknowledgments**

One of us (S. A.) gratefully acknowledges the Physics Department of Middle East Technical University for warm hospitality extended to him during his visits. We thank R. Machleidt for providing a table of their cross-sections, and P. Shuck for fruitful discussions. This work is supported in part by the U.S. DOE Grant No. DE-FG05-89ER40530.

## REFERENCES

- [1] J. Speth (Ed.), Electric and Magnetic Giant Resonances in Nuclei, World Scientific (1991).
- [2] G. F. Bertsch, R. A. Broglia, Oscillations in Finite Quantum Systems, Cambridge (1994).
- [3] J. Wambach, Rep. Prog. Phys. **51** (1988) 989.
- [4] G. F. Bertsch, P. F. Bortignon, R. A. Broglia, Rev. Mod. Phys. **55** (1983) 287.
- [5] P. F. Bortignon, R. A. Broglia, G. F. Bertsch, and J. Pacheco, Nucl. Phys. **A460** (1986) 149.
- [6] W. E. Ormand, P. F. Bortignon, R. A. Broglia, Phys. Rev. Lett. **77** (1996) 607.
- [7] D. Kusnezov, Y. Alhassid and K. A. Snover, Phys. Rev. Lett. **81** (1998) 542.
- [8] S. Ayik, Phys. Lett. **B493** (2000) 1.
- [9] M. Belkacem, S. Ayik, A. Bonasera, Phys. Rev. **C52** (1995) 2499.
- [10] S. Ayik, O. Yilmaz, A. Gokalp, P. Schuck, Phys. Rev. **C58** (1998) 1594.
- [11] U. Furmann, K. Morawetz, R. Welke, Phys. Rev. **C58** (1998) 1473.
- [12] D. Lacroix, P. Chomaz, S. Ayik, Phys. Rev. **C58** (1998) 2154; Phys. Lett. **B489** (2000) 137.
- [13] A. Smerzi, A. Bonasera, M. diToro, Phys. Rev. **C44** (1991) 1713.
- [14] V. Baran et al., Nucl. Phys. **A599** (1996) 29c.
- [15] V. M. Kolomietz, V. A. Plujko and S. Shlomo, Phys. Rev. **C54** (1996) 3014.
- [16] M. G. Q. Li, R. Machleidt, Phys. Rev. **C48** (1993) 1702; **C49** (1994) 566.
- [17] O. Yilmaz, A. Gokalp S. Yildirim, S. Ayik, Phys. Lett. **B472** (2000) 258.

- [18] Y. Abe, S. Ayik, P. G. Reinhard, E. Suraud, Phys. Rep. **275** (1996) 49.
- [19] S. Ayik, D. Lacroix, P. Chomaz, Advances in Nuclear Dynamics, **5**, W. Bauer (Ed.), Plenum, New York (1999); Phys. Rev. **C61** (1999) 014608.
- [20] R. Hasse, in Proceedings of Phase Space Approach to Nuclear Dynamics, eds. M. diToro, W. Norenberg, M. Rosina and S. Stringari, World Scientific, Singapore (1985).
- [21] J. P. Blaizot, Phys. Rep. **64** (1980) 171.
- [22] V. Abrosimov, M. diToro, A. Simerzi, Z Phys.**A347** (1994) 161.
- [23] J. M. Eisenberg, W. Greiner, Nuclear Models, North Holland, Amsterdam (1970).
- [24] P. Schuck et al., Prog. Part. Nucl. Phys. Vol. **22**(1989) 181.
- [25] P. Ring, P. Schuck, The Nuclear Many Body Problem, Springer, Berlin (1980).

## Figure Captions:

**Figure 1:** The spin-isospin averaged nucleon-nucleon in-medium cross-sections as a function of bombarding energy  $E_{lab}$  at several different densities. Dotted lines are cross-sections of Li and Machleidt, and solid and dashed lines are cross-sections associated with the SkM\* and the Gogny forces with the bare nucleon mass (left) and the effective nucleon mass (right), respectively.

**Figure 2:** The spin-isospin averaged nucleon-nucleon in-medium cross-sections as a function of density  $\rho$  at  $E_{lab} = 100 MeV$ . Dotted lines are cross-sections of Li and Machleidt, and solid and dashed lines are cross-sections with the SkM\* and the Gogny forces with the bare nucleon mass (left) and the effective nucleon mass (right), respectively.

**Figure 3:** The collisional damping width of giant monopole resonance in  $^{120}Sn$  and  $^{208}Pb$  as a function of temperature. Dotted lines are calculations with the cross-sections of Li and Machleidt, and solid and dashed lines are results with the SkM\* and the Gogny cross-sections with the bare nucleon mass (lower panel) and the effective nucleon mass (upper panel).

**Figure 4:** The collisional damping width of giant quadrupole resonance in  $^{120}Sn$  and  $^{208}Pb$  as a function of temperature. Dotted lines are calculations with the cross-sections of Li and Machleidt, and solid and dashed lines are results with the SkM\* and the Gogny cross-sections with the bare nucleon mass (lower panel) and the effective nucleon mass (upper panel). For distortion factors fluidynamical model is used.

**Figure 5:** The collisional damping width of giant quadrupole resonance in  $^{120}Sn$  and  $^{208}Pb$  as a function of temperature. Dotted lines are calculations with the cross-sections of Li and Machleidt, and solid and dashed lines are results with the SkM\* and the Gogny cross-sections with the bare nucleon mass (lower panel) and the effective nucleon mass (upper panel). For distortion factors scaling approximation is used.

**Figure 6:** The collisional widths of giant monopole (left) and giant quadrupole (right) vibrations as a function of the mass number at zero temperature with effective nucleon mass. Experimental widths are shown by solid dots with error bars.

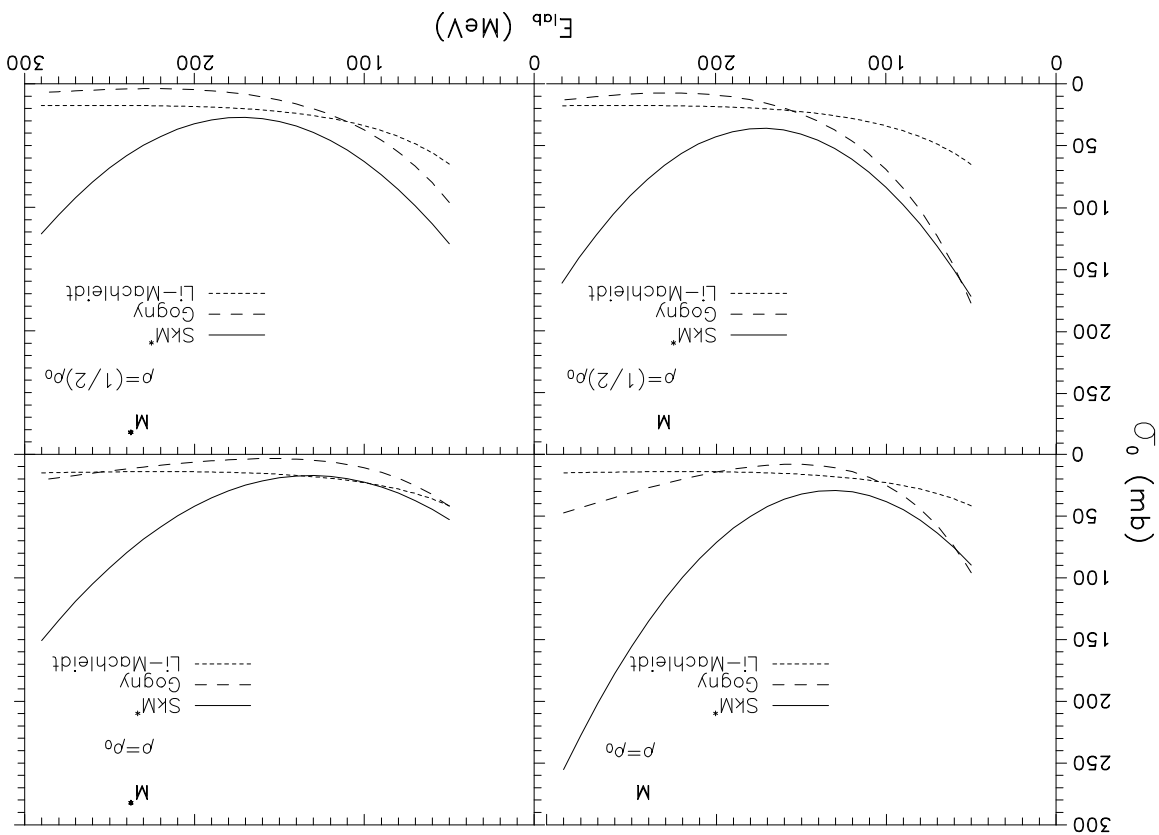


Figure 1

Figure 2

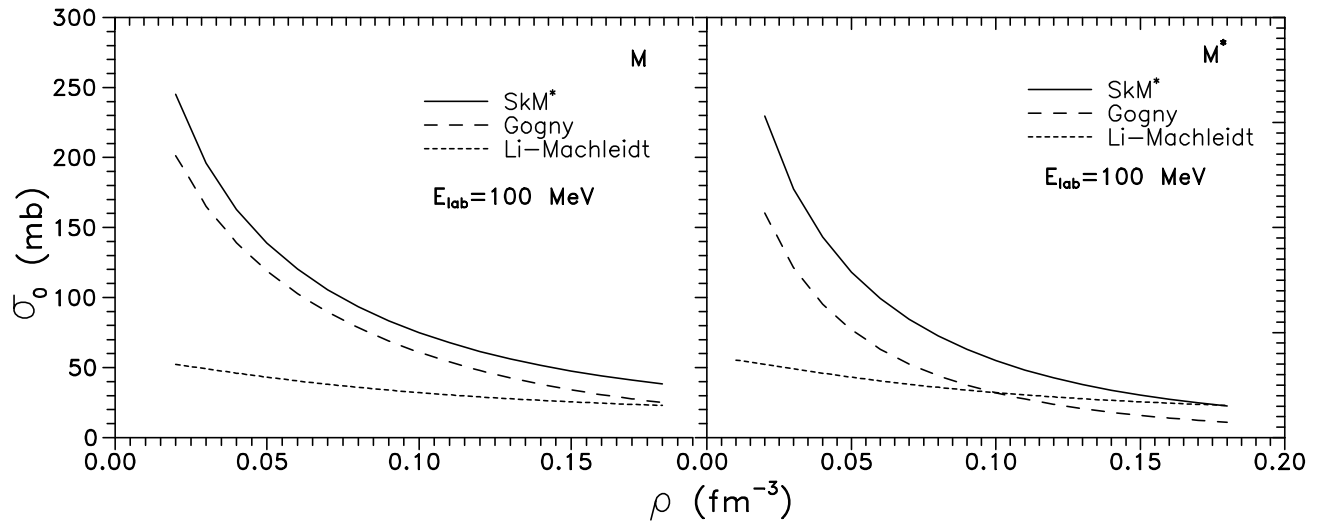


Figure 3

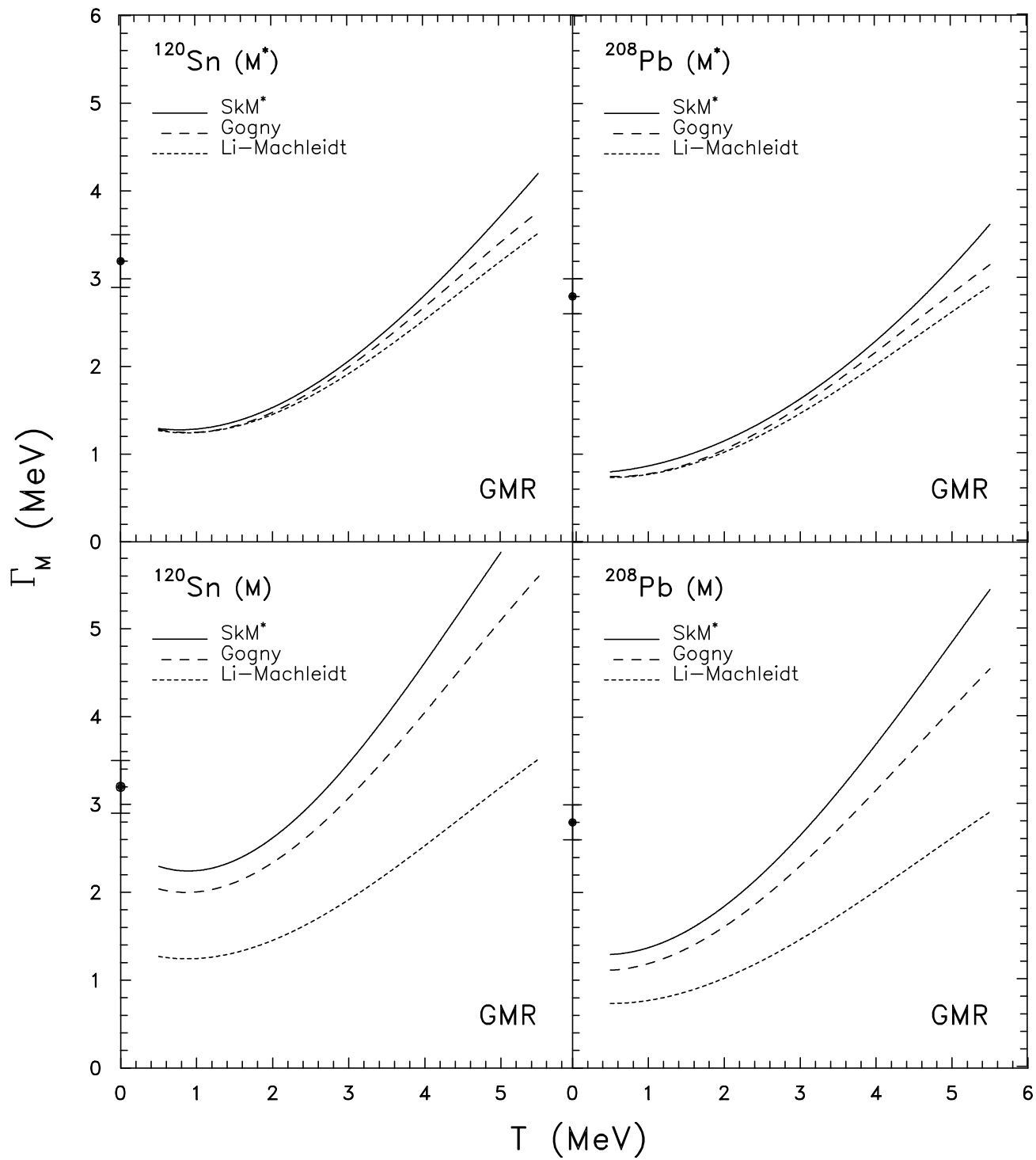


Figure 4

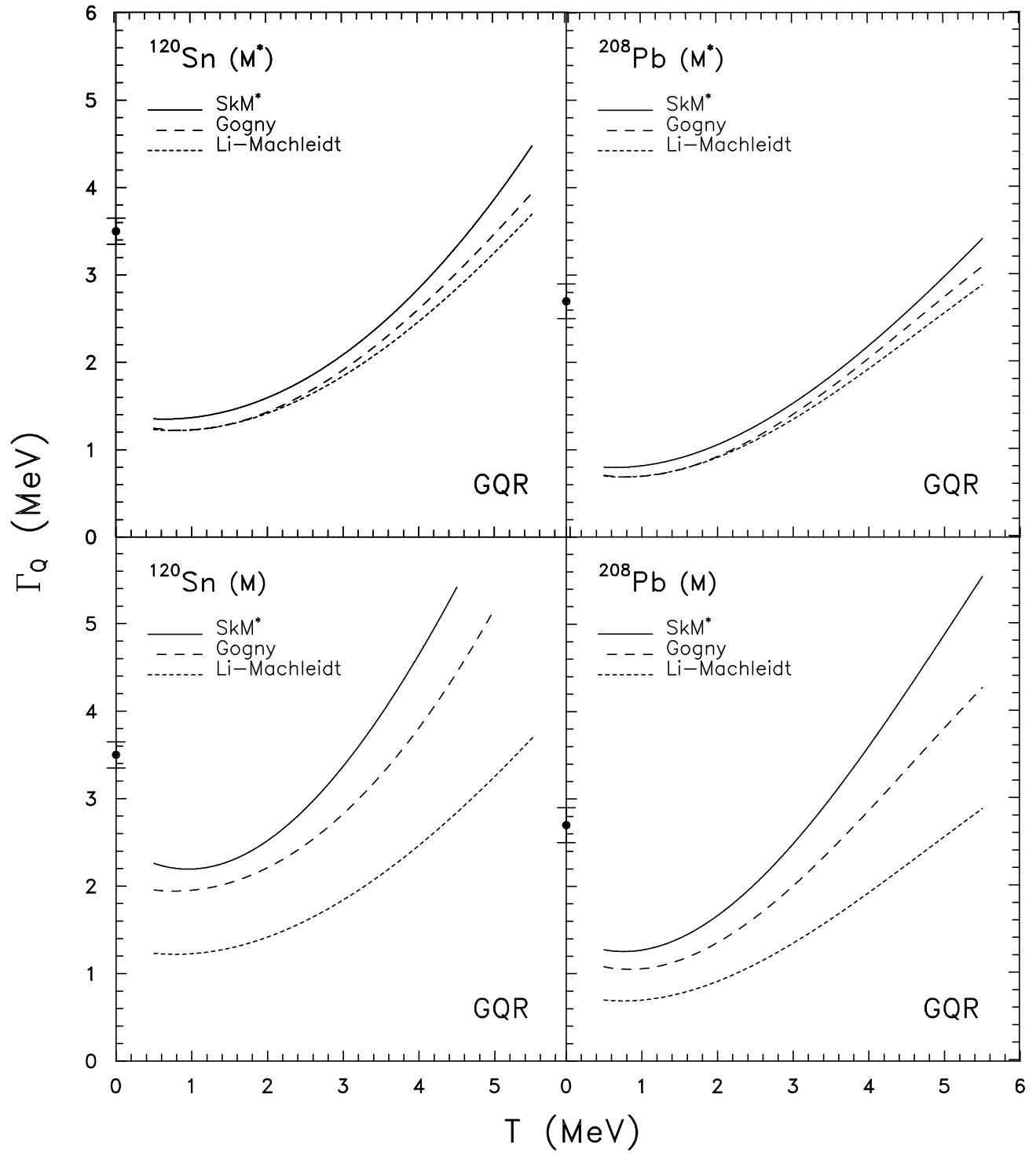


Figure 5

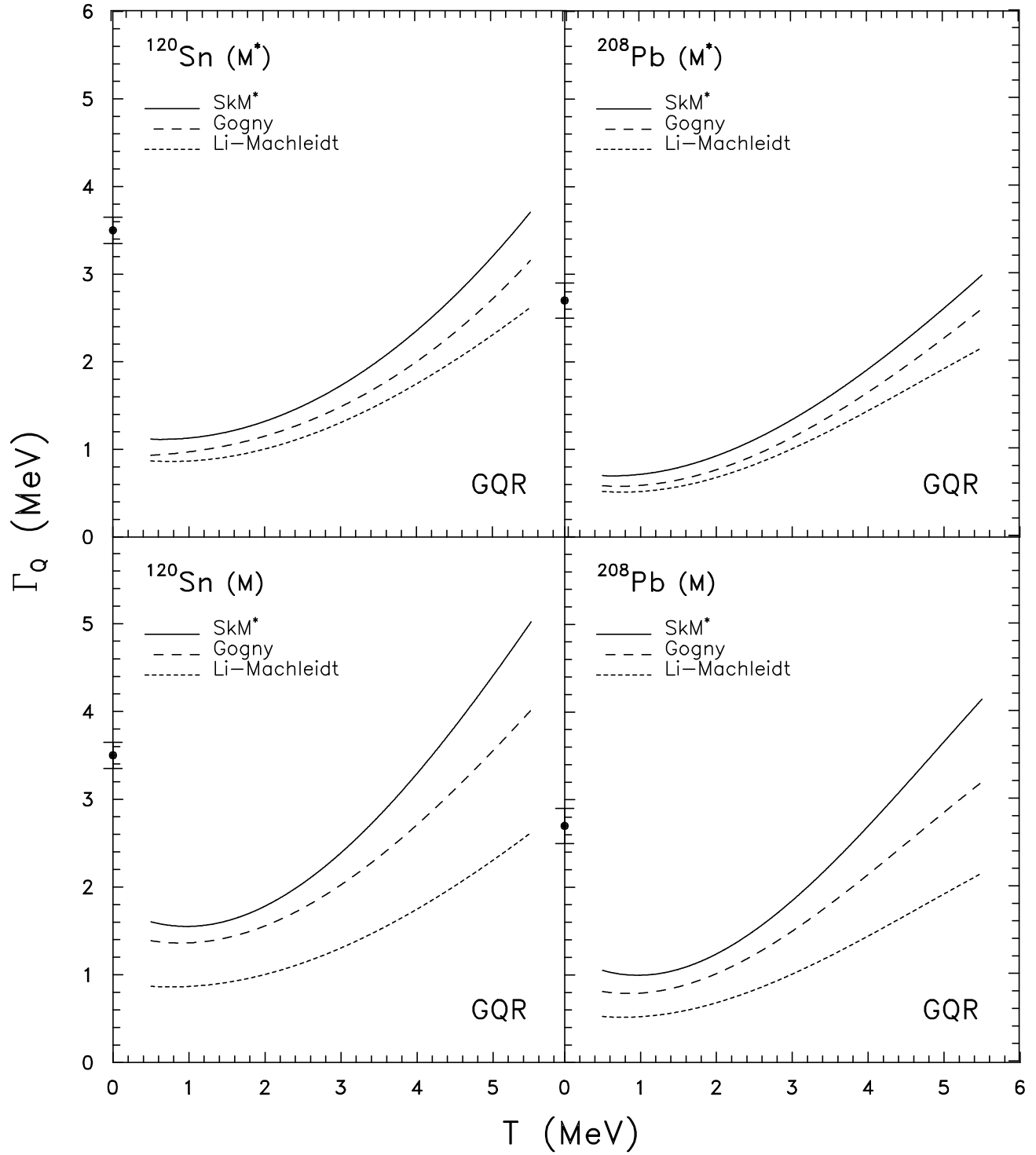


Figure 6

